

Low-energy proton capture reactions in the mass region 55-60

Saumi Dutta,^{*} Dipti Chakraborty,[†] G. Gangopadhyay,[‡] and Abhijit Bhattacharyya[§]

*Department of Physics, University of Calcutta
92, Acharya Prafulla Chandra Road,
Kolkata-700 009, India*

Low energy proton capture reactions in the mass 55-60 region are studied in a microscopic optical model. Nuclear density profile is calculated using the relativistic mean field theory. The DDM3Y interaction is folded with the theoretical density to obtain the proton-nucleus optical potential. A definite set of normalization parameters has been obtained for the concerned mass region by comparing with all available experimental data in this mass region. These parameters have been used to obtain proton capture rates for astrophysically important reactions in this mass region.

PACS numbers: 24.10.Ht, 25.40.Cm, 25.40.Lw, 25.40.Kv

I. INTRODUCTION

The study of the role of individual nuclear reactions in stellar evolution has been an important field of research in the last few decades. As a star evolves with time it passes through burning in different ranges of nuclear mass. At the same time, different nuclear processes become important at different time periods of evolution. A comprehensive study of these processes sheds light on various astrophysical phenomena.

There are certain astrophysical sites which are responsible for the production of heavier nuclei beyond iron through the rapid capture of protons on seed nuclides. In the mass region of our interest there are certain proton rich naturally occurring nuclei, which are not produced by the r -process or the s -process. These are called p -nuclei. Proton capture reactions in certain astrophysical sites can account for the formation of some of these proton rich nuclides. For example x-ray bursters with a large proton flux in the peak temperature around 1-3 GK are suitable astrophysical sites for the production of certain nuclei. To find out the abundance of different nuclei as well as the evolution of the process in these sites a network calculation is necessary which involves a large number of reactions.

It is thus imperative to calculate the rates and/or cross sections of these reactions in different mass ranges. Our group has already calculated the cross sections and hence

the astrophysical S-factors in the mass range $A = 60 - 100$ [1–4]. Some implications of the new rates has also been investigated in the context of rp-process [5, 6]. In the present work, we extend our calculation to the $A = 55 - 60$ region.

The rp-process is sensitive to a number of reactions in this region. The most challenging aspect to look at in these scenarios is that most of the nuclei involved in those reactions are not produced in the laboratory. For example, Parikh *et al.* [7] have identified proton capture reactions on ^{56}Ni and $^{57,59}\text{Cu}$ targets as important in the rp-process in certain scenarios. However, experimental rates are not available for these reactions because stable targets do not occur in nature. Hence, one has to depend on theoretical calculations in this domain.

In explosive proton rich environments, such as x-ray bursts, proton capture has to compete with its inverse, *i.e.* photo-disintegration. This competition results in waiting points and causes delay of further nucleosynthesis. With temperature, pressure and proton mass fractions being different at different regions of these sites as well as being time-varying quantities, incorporation of all these physical conditions in the nuclear network is a big challenge. Rauscher *et al.* [8, 9] have calculated the rates for various proton, neutron and α -particle induced reactions and their reverse reactions in Hauser-Feshbach formalism for targets with wide range of atomic numbers and masses and for a wide range of temperature. Theoretical calculations in this mass region essentially utilize the Hauser-Feshbach formalism where, the optical model potential, a key ingredient, is often taken in a local or a global form. However, a more microscopic approach is also possible using an optical potential constructed utilizing nuclear densities. If the target is stable, nuclear

^{*}Electronic address: saumidutta89@gmail.com

[†]Electronic address: diptichakraborty2011@gmail.com

[‡]Electronic address: ggphy@caluniv.ac.in

[§]Electronic address: abphy@caluniv.ac.in

density is available through electron scattering. However, in the absence of a stable target, theory remains our sole guide to describing the density. It is imperative to test the theoretical calculations, where experimental data are available, to verify its applicability. We aim to check the success of microscopic optical potentials based on mean-field densities in explaining the available reaction cross sections in this mass region. A good description depending essentially on theory will allow one to extend the present method to the critical reactions, which are beyond present day laboratory capabilities.

A well defined nucleon-nucleon (NN) interaction is of major importance for microscopic calculation of nucleon-nucleus and nucleus-nucleus potentials used in the theoretical analysis of different reactions as well as scattering. The optical model potential is highly successful for explanation of different branches of nuclear reaction. It can reliably predict the basic observables such as total and partial cross sections, elastic scattering angular distributions, etc, even for those target nuclei and for those energy regions for which no experimental data exist. We have used the density dependent M3Y interaction by folding the potential with target radial matter densities. This interaction has been used in many calculations and has given satisfactory results.

The paper is organized as follows. In the next section, we outline our method of calculation. Essentially we construct an optical model potential through folding an NN interaction with the theoretical density profile. For this purpose we use the relativistic mean field (RMF) theory to obtain the density profile of the targets. In Sec. III the results of our work are discussed in detail. Finally we summarize our work.

II. MODEL CALCULATION

The RMF approach has proved to be very successful in describing various nuclear properties such as binding energy of nuclei in ground states as well as excited states, nuclear density profile, rms charge radii, deformation, nuclear halo, moment of inertia, etc [10]. It is considered to be the relativistic generalization of the non-relativistic models such as Gogny force or Skyrme force Hartree-Fock theory using effective mesonic degrees of freedom rather than instantaneous forces. The model is basically based upon two major approximations namely mean-field approximation and no-sea approximation [11]. The starting point of RMF is a suitable Lagrangian density that includes the coupling between the nucleon field and

meson field as well as meson self couplings so that the Lagrangian can successfully describe the properties of finite nuclei as well as the equation of state (EOS) of nuclear matter. There are different variations of Lagrangian density as well as different parameterizations. An accurately calibrated relativistic Lagrangian density, FSUGold [12], has been fitted to the charge radii of nuclei. It contains two additional parameters, compared to conventional RMF models, describing self coupling of vector-isoscalar meson and coupling between the vector-isovector meson and vector-isoscalar meson. These two additional parameters significantly affect the softening of the EOS, the accurate determination of which is needed for the study of various nuclear properties such as charge radii, masses, etc.

Thus theoretical density profiles are extracted in the RMF approach considering the FSUGold interaction. The charge density is obtained by convoluting the point proton density considering the finite size of the nucleus.

$$\rho_{ch}(\mathbf{r}) = e \int \rho(\mathbf{r}')g(\mathbf{r} - \mathbf{r}')d\mathbf{r}' \quad (1)$$

where $g(r)$ is the Gaussian form factor given by,

$$g(r) = (a\sqrt{\pi})^{-3} \exp(-r^2/a^2) \quad (2)$$

where a is a constant whose value is assigned to 0.8 fm. Using the nuclear density profile we have numerically obtained rms charge radii.

While calculating the charge density or the radius, no attempt has been made to take the correction due to center of mass into account. Calculations on harmonic oscillator wave functions show that the correction is small for heavier nuclei. For example, Quentin has shown[13] that the effect of inclusion of center of mass correction in the radius is given by $\delta r/r \approx 0.9/A^{4/3}$. Hence, we do not expect the density profile to be affected significantly due to this approximation.

The M3Y interaction [14, 15] is based on a realistic G-matrix which in turn is constructed in a harmonic oscillator representation averaging over a range of energies as well as densities. It has no explicit density dependence nor energy dependence. Although in most cases these averages do not matter producing satisfactory results, in few cases it becomes necessary to incorporate explicit density dependence into M3Y interaction and then it is named as density dependent M3Y (DDM3Y) effective interaction [16]. Low energy proton capture reactions are highly sensitive to nuclear radius as well as density. In the present work we have used density de-

pendent M3Y Reid-Elliot effective nucleon-nucleon interaction within a folding model prescription [2]. The density dependence is incorporated in the same way as suggested in Refs. [17, 18].

Further, we have included a spin-orbit term into the potential considering Scheerbaum prescription [19] which has been coupled with the phenomenological complex potential depths. These depths are functions of energy which are assigned standard values as in Lahiri *et al.* [2]. These values are kept unaltered throughout our present work.

We have incorporated the density dependent M3Y interaction within the TALYS1.4 code [20] and performed a Hauser-Feshbach (HF) calculation. We have chosen Goriely's microscopic level densities and Hartree Fock Bogolyubov model for $E1$ γ -ray strength function. As seen in our previous calculations [2, 4], these choices can explain the experimental results more accurately. All these options are available in the code. We have also included the effect of the width fluctuation correction which has a significant impact at low incident energies. Up to 30 discrete levels are included for both target and residual nuclei, which are considered in Hauser-Feshbach decay and γ -ray cascade. We also include a maximum of 30 discrete levels for the nuclei resulting from binary emission in Hauser-Feshbach decay and γ -ray cascade. HF calculations are done with full j, l coupling. We have incorporated the density data obtained from RMF approach to obtain the optical model potential.

Because of rapid variation of cross-section with energy in the low energy region, it is difficult to compare the theory and experiment. A standard alternative way is to compare another important quantity instead of cross-section, namely astrophysical S-factor [21].

The proton capture reactions in astrophysical sites occur within a narrow energy window [21]. This effective energy window approximately of Gaussian shape around a peak (known as Gamow peak) is known as Gamow window. The expressions for the Gamow peak and Gamow width in a practical form are given respectively as,

$$E_0 = 0.1220(Z_t^2 Z_p^2 \mu T_9^2)^{1/3} \text{ MeV} \quad (3)$$

$$\Delta = 0.2368(Z_p^2 Z_t^2 \mu T_9^5)^{1/6} \quad (4)$$

where μ is the reduced mass and T_9 denotes the temperature in GK. Thus most of the astrophysically important reactions occur within a narrow energy window $E_0 - \Delta/2$ to $E_0 + \Delta/2$. We see that for (p, γ) reactions on stable isotopes in the mass range 55-60, the Gamow window lies

between 1 MeV to 3 MeV for temperature around 3 GK. Hence, we have carried out our calculation in this low energy window and compared our results with the measured data where available. In calculating the Gamow peak, Gamow width and hence Gamow window we have taken the masses from Audi *et al.* [22].

III. RESULTS

Because the optical model is dependent on the density profile of the nucleus, we calculate the density and the charge radii of nuclei in this mass region using RMF formalism. The theoretical density values are plotted as a function of radius and compared with available experimental values in Fig. 1. As can be seen the agreement is extremely good. The experimental data are taken from Wohlfahrt *et al.* [23].

We also compare all the available rms charge radii values with theoretical results in table I. The experimental values are taken from Angeli *et al.* [24]. It can be seen that the RMF calculation has an excellent predictive power, the relative difference between theory and experiment in all cases being less than 0.5%.

TABLE I: Charge radii of various nuclei extracted in the RMF approach compared with measured values from Angeli *et al.* [24]

Nucleus	Charge radius(fm)	
	Theory	Experiment.
⁵⁵ Mn	3.7057	3.7057
⁵⁶ Mn	3.7189	3.7146
⁵⁶ Fe	3.7361	3.7377
⁵⁷ Fe	3.7497	3.7532
⁵⁸ Fe	3.7634	3.7745
⁵⁹ Co	3.7924	3.7875
⁵⁸ Ni	3.7916	3.7757
⁶⁰ Ni	3.8193	3.8118

We have tried to set a definite normalization for the optical model potential that fits all the reaction data in the concerned mass region. The potential obtained by folding has been multiplied by the normalization constant 2.0 to get the real part of the potential. The DDM3Y interaction does not have any imaginary part. We have multiplied the folding potential by the normalization constant 1.4 to obtain the imaginary part of the optical potential. These final parameters have been ob-

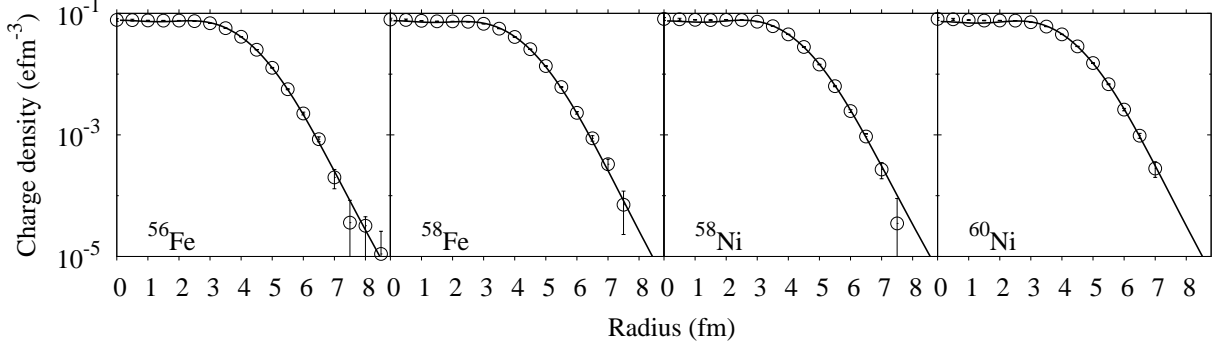


FIG. 1: Theoretical density profile of various nuclei in mass 55-60 region from RMF approach compared with experimental data obtained by elastic electron scattering taken from Wohlfahrt et. al. [23]. The solid lines denote the theoretical result and discrete points with error-bars represent the experimental data. In most of the cases, especially for lower radii values, the errors associated are smaller than the dimension of the empty circles.

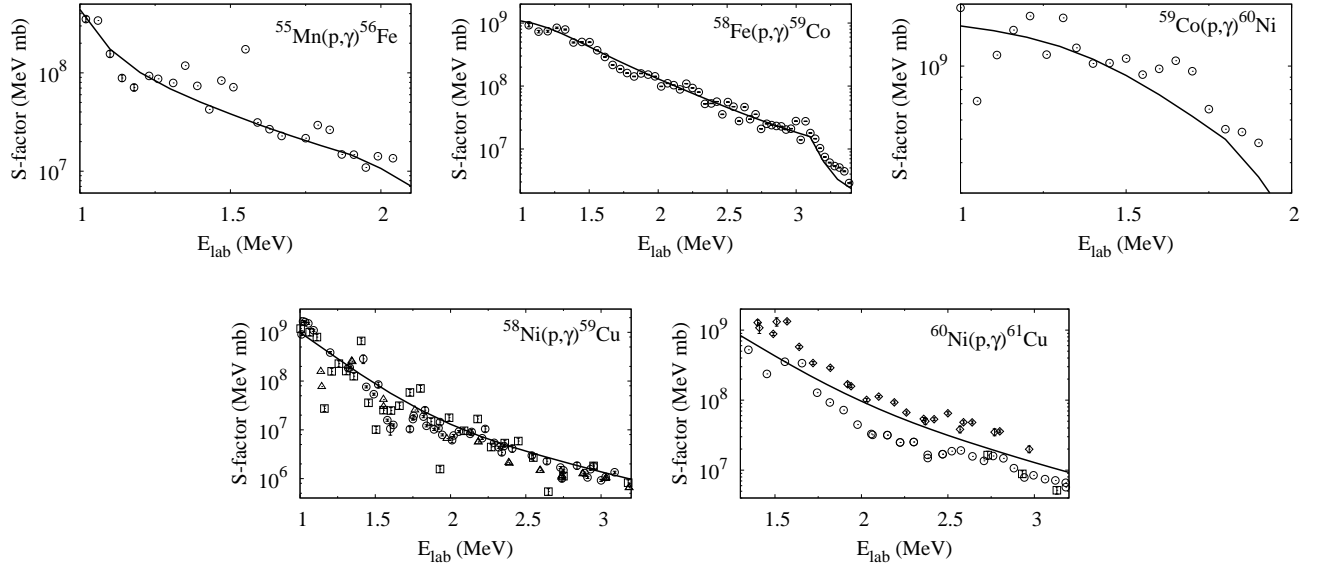


FIG. 2: Comparison of theoretical astrophysical S-factor calculations in the present work with experimental data for proton capture on (a) ^{55}Mn , (b) ^{58}Fe , (c) ^{59}Co , and (d) ^{58}Ni , (e) ^{60}Ni . See text for the explanation of different symbols and the Supplemental Material in Ref. [25] for numerical values of S-factor.

tained after many trials to ensure a reasonable agreement with experimental data for all the known low energy proton capture reactions in the mass region of our interest. Although a single normalization can not reproduce the

experimental data excellently for all reactions in the region, *i.e.* each individual reaction may have different normalization for best matching with measurement, it is necessary to consider a single definite normalization to

extend the work to unknown nuclei in the mass region for which no experimental data exist. We note that the fitted parameters for the present mass range differ from the neighbouring mass region in our earlier calculation. This is possibly due to the fact that the mass selected in the present calculation is lighter than our previous regions. Possibly, the larger depths of the potential is required to adjust for the low mass region.

The comparison of S-factors obtained after incorporating DDM3Y interaction using the above normalization constants with experimental data are shown in fig. 2. The numerical values of the S-factors and the reaction rates are given in Supplemental Material [25]. The experimental data are taken from Ref [26–28] for ^{55}Mn , ^{58}Fe and ^{59}Co , respectively. For ^{58}Ni and ^{60}Ni , experimental data are taken from Refs. [29–31] and Refs. [30, 32, 33], respectively. In many cases the experimental data are very old. Errors are also not available in some cases. For ^{55}Mn , ^{58}Fe and ^{59}Co , circles represent the experimental data. For ^{58}Ni , triangles, squares and circles represent the data from Refs. [29–31], respectively. For ^{60}Ni there are three different sources of data [30, 32, 33] which are denoted by squares, circles and diamonds, respectively.

In all cases the solid line denotes the theoretical DDM3Y result. In ^{55}Mn , there are certain ambiguities in experimental data, especially in the energy range between 1.3 to 1.6 MeV. The experiment was done using Ge(Li) detector by integrated beam current method more than three decades ago. However, errors are not associated with most of the data points. Only four data points in the energy range of our interest have errors associated with those.

Our calculations give an excellent description of experimental data for ^{58}Fe . The experiment for ^{58}Fe was done using Ge(Li) detector and the data was compared with statistical model predictions [27]. For ^{59}Co again there are large fluctuations in experimental data. Butler *et al.* [28] stated that they had observed several resonances in the reaction $^{59}\text{Co}(p, \gamma)^{60}\text{Ni}$ but the resonances were too close to be resolved clearly.

Our calculation for ^{58}Ni overpredicts the measurement of Tingwell *et al.* [31] by a factor of ~ 2.5 , approximately. This experiment was carried out by both beam current integrated method and single target irradiation method using Ge(Li) detector. Tingwell *et al.* also compared their data with statistical model calculations. They found that their statistical calculation overestimates the measurement by a factor of ~ 2.5 for ^{58}Ni , which agrees with our results. Cheng *et al.* [29] also

measured cross section for this reaction using the activation technique. Except in the energy range ~ 1.4 -1.8 MeV, where the measurement itself has large discrepancies, the data agree more or less well with our theoretical calculations.

For the reaction $^{60}\text{Ni}(p, \gamma)^{61}\text{Cu}$, Tingwell *et al.* themselves compared the experimental results with the statistical model predictions and showed that normalizing the optical model imaginary well depth for Ni isotopes by a factor of 1.5 leads to a better agreement between theory and experiment [33]. Our calculation, in the case of ^{60}Ni , overpredicts the experimental data of Tingwell *et al.* [33] by a factor ~ 1.5 , whereas it underpredicts the data of Krivosov *et al.* [30] by a factor ~ 0.35 .

With the above normalization, we have calculated the rates for (p, γ) reactions identified as important by Parikh *et al.* [7]. The calculated rates are compared with NON-SMOKER [8, 9, 34] rates. The NON-SMOKER results are from a HF calculation based on masses from experimental measurements and calculation in the Finite Range Droplet Model [35]. Other details of the calculation can be obtained from the references. The results have been plotted in figure 3. We see that in the range 1-4 GK, the NON-SMOKER results differ from the present calculations significantly. For the $^{56}\text{Ni}(p, \gamma)$ reaction, although the results agree at low temperature, at higher temperature the NON-SMOKER rates are larger. On the other hand, for the other two reactions, *viz.* $^{57}\text{Cu}(p, \gamma)$ and $^{59}\text{Cu}(p, \gamma)$, our calculation predicts a significantly larger rate throughout the temperature range. It will be interesting to see the effects of these results on astrophysical scenarios.

IV. SUMMARY

Low energy (p, γ) reactions are studied in a semi-microscopic approach in the HF formalism and compared with experiments in the mass region 55-60. Radial density profiles are obtained using the RMF approach and are folded with the DDM3Y NN interaction to obtain semi-microscopic optical potentials. Both the real and imaginary depths of the potential are normalized to obtain a good agreement between theory and experiment. The S-factors for (p, γ) reactions are evaluated in the Gamow window corresponding to 3 GK. We have not modified the parameters to fit individual reactions as our aim is to construct a framework for calculation of astrophysical reactions involving unstable nuclei. Rates for important astrophysical reactions calculated

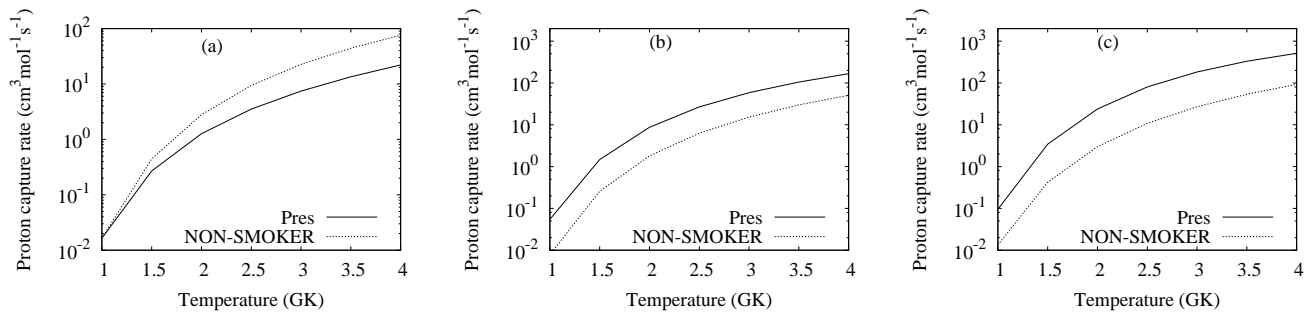


FIG. 3: Comparison of astrophysical rates from the present calculation with NON-SMOKER results from Rauscher *et al.* [8, 9] for the reactions (a) $^{56}\text{Ni}(p, \gamma)^{57}\text{Cu}$, (b) $^{57}\text{Cu}(p, \gamma)^{58}\text{Zn}$ and (c) $^{59}\text{Cu}(p, \gamma)^{60}\text{Zn}$. See text for details and the Supplemental Material in Ref. [25] for numerical values of rates.

in the present approach differ significantly from NON-SMOKER rates. The key feature of our work is that we have taken all nuclei in the same footing and same methodology has been used for all of them to avoid systematic error.

Acknowledgment

The authors acknowledge the financial support provided by UGC(DRS), DST and the University of Cal-

cutta.

-
- [1] G. Gangopadhyay, Phys. Rev. C **82**,027603 (2010).
 - [2] C. Lahiri and G. Gangopadhyay, Eur. Phys. J. A **47**, 87 (2011).
 - [3] C. Lahiri and G. Gangopadhyay, Phys. Rev. C **84**, 057601 (2011).
 - [4] C. Lahiri and G. Gangopadhyay, Phys. Rev. C **86**, 047601(2012).
 - [5] C. Lahiri and G. Gangopadhyay, Int. J. Mod. Phys. E **21**, 1250074 (2012).
 - [6] C. Lahiri and G. Gangopadhyay, Mod. Phys. Lett. A **28**, 1350076 (2013).
 - [7] A. Parikh, J. José, F. Moreno and C. Iliadis, New Astron.Rev. **52**, 409 (2008).
 - [8] T. Rauscher, F. K. Thielemann, At. Data Nucl. Data Tables **75**,1 (2000).
 - [9] T. Rauscher, F. K. Thielemann, At. Data Nucl. Data Tables **79**, 47, (2000)
 - [10] P. Ring, Prog. Part. Nucl. Phys. **37**, 193 (1996).
 - [11] Horst Müller and Brian D. Serot, Nucl. Phys. **A606**, 508 (1996).
 - [12] B. G. Todd-Rutel and J. Piekarewicz, Phys. Rev. Lett. **95**, 122501 (2005).
 - [13] P. Quentin, in Nuclear Self-Consistent Fields, edited by G. Ripka and M. Porneuf (North-Holland/ American Elsevier, 1975) p 297.
 - [14] G. Bertsch, J. Borysowicz, H. McManus, and W.G. Love, Nucl. Phys. **A284**, 399 (1977).
 - [15] G.R. Satchler and W.G. Love, Phys. Rep. **55**, 183 (1979).
 - [16] M.D. Myers, Nucl. Phys. **A204**, 465 (1973).
 - [17] D.N. Basu, P. Roy Chowdhury, C. Samanta, Phys. Rev. C **72**, 051601 (2005).
 - [18] D.N. Basu, J. Phys. G:Nucl. Part. Phys. **30**, B7 (2004).
 - [19] R. R. Scheerbaum, Nucl. Phys. **A257**, 77 (1976).
 - [20] A. J. Koning S. Hilaire, and M. Duizvestijn, Proceedings of the International Conference on Nuclear Data for Science and Technology, April 22-27, 2007, Nice, France, edited by O. Bersillon, F. Gunsing, E. Bauge, R. Jacqmin, S. Leray (EDP Sciences, 2008) p. 211.
 - [21] C. E. Rolfs and W. S. Rodney, Cauldrons in the Cosmos, The University of Chicago Press, Chicago and London, 1988.
 - [22] G. Audi and A. H. Wapstra, Nucl. Phys. **A729**, 129

- (2003).
- [23] H. D. Wohlfahrt, O. Schwentker, G. Fricke, H. G. Anderson, E. B. Shera, Phys. Rev. C **22**, 264 (1980).
- [24] I. Angeli, K.P. Marinova, At. Data. and Nucl. Data Tables **87**, 185 (2004).
- [25] See Supplemental Material at [URL will be inserted by publisher] for numerical values of calculated S -factors and reaction rates.
- [26] L. W. Mitchell, D. G. Sargood, Aust. J. Phys. **36**, 1 (1983).
- [27] S. G. Tims, A. F. Scott, A. J. Morton, V. Y. Hansper, and D. G. Sargood, Nucl.Phys. **A563**, 473 (1993).
- [28] J. W. Butler, C. R. Gossett, Phys. Rev. **108**, 1473 (1957).
- [29] C.W. Cheng, J. D. King, Can. J. Phys. **58**, 1677 (1980).
- [30] G.A. Krivonosov *et al.*, Izv. Akad. Nauk SSSR, Ser. Fiz. **41**, 2196(1977).
- [31] C.I.W. Tingwell, L. W. Mitchell, M. E. Sevier and D. G. Sargood, Nucl.Phys. **A439**, 371(1985).
- [32] A. Simon *et al.*, Phys. Rev. C **87**, 055802 (2013).
- [33] C.I.W. Tingwell *et al.*, Nucl. Phys. **A496**, 127 (1989).
- [34] <http://nucastro.org/nonsmoker.html>
- [35] J.R. Nix, W.D. Myers, and W. Swiatecki, At. Data Nucl. Data Tables **59**, 185 (1995).